Fabrication of Electroactive Layer-by-Layer Films of Myoglobin with Gold Nanoparticles of Different Sizes

Hong Zhang,[†,‡] Haiyun Lu,[†] and Naifei Hu*[,†]

Department of Chemistry, Beijing Normal University, Beijing 100875, P. R. China, and Department of Chemistry, Fuyang Teachers College, Fuyang 236400, P. R. China

Received: September 19, 2005; In Final Form: December 13, 2005

Alternate adsorption of oppositely charged myoglobin (Mb) and gold nanoparticles with different sizes were used to assemble $\{Au/Mb\}_n$ layer-by-layer films on solid surfaces by electrostatic interaction between them. The direct electrochemistry of Mb was realized in $\{Au/Mb\}_n$ films at pyrolytic graphite (PG) electrodes, showing a pair of well-defined, nearly reversible cyclic voltammetry (CV) peaks for the Mb heme Fe^{III}/Fe^{II} redox couple. Quartz crystal microbalance (QCM), electrochemical impedance spectroscopy (EIS), and CV were used to monitor or confirm the growth of the films. Compared with other Mb layer-by-layer films with nonconductive nanoparticles or polyions, $\{Au/Mb\}_n$ films showed much improved properties, such as smaller electron-transfer resistance (R_{ct}) measured by EIS with $Fe(CN)^{3-/4-}$ redox probe, higher maximum surface concentration of electroactive Mb (Γ^*_{max}), and better electrocatalytic activity toward reduction of O_2 and H_2O_2, mainly because of the good conductivity of Au nanoparticles. Because of the high biocompatibility of Au nanoparticles, adsorbed Mb in the films retained its near native structure and biocatalytic activity. The size effect of Au nanoparticles on the electrochemical and electrocatalytic activity of Mb in $\{Au/Mb\}_n$ films was investigated, demonstrating that the $\{Au/Mb\}_n$ films assembled with smaller-sized Au nanoparticles have smaller R_{ct}, higher Γ^*_{max}, and better biocatalytic reactivity than those with larger size.

1. Introduction

Study on the direct electrochemistry of redox proteins is of theoretical and practical significance in biology, analytical chemistry, and other fields of science, which would provide a model for the mechanistic study of electron transfer among enzymes in real biological systems and establish a foundation for fabricating the third-generation biosensors without using mediators.[1,2] After realizing that the redox proteins in solution are usually difficult to exchange electrons directly with naked solid electrodes, more researchers are now attempting to incorporate the proteins into ultrathin films modified on electrode surface, and the direct electrochemistry of proteins in various films attract an increasing research interest. Such films may provide a suitable microenvironment for the proteins and facilitate the electron exchange between the proteins and underlying electrodes.[3]

There are various methods to prepare protein films, among which the layer-by-layer assembly is relatively new and developed very rapidly in recent years. The idea of layer-by-layer assembly is originally from the alternate adsorption of oppositely charged polyelectrolytes on solid surfaces,[4,5] and recently extended to fabricate multilayered protein films.[6,7] Particularly, since inorganic nanoparticles have their unique properties, they are also used to assemble layer-by-layer films with proteins. The proteins in the multilayer films with nanoparticles exhibit direct and reversible cyclic voltammetry (CV) responses at underlying electrodes, as several examples demonstrated.[8−11] Compared with other methods for film preparation, the layer-by-layer assembly has advantages in its flexibility, simplicity, and the precise control of film component and layer thickness.

Gold nanoparticles, also called gold colloids, are the most stable metal nanoparticles and have some unique properties, such as high biocompatibility, good conductivity, and distinctive size-related electronic and optical behaviors. Au colloids are thus applied to various fields, especially in nanoscience and nanotechnology, and will become key materials and building blocks in the 21st century.[12] Au nanoparticles are also used to immobilize redox proteins on electrode surface, and the direct electrochemistry of proteins have been realized.[13] For example, reversible electrochemistry of cytochrome *c* (Cyt *c*) in solution was obtained at SnO_2 electrodes modified with colloidal Au.[14] Chen and co-workers immobilized horseradish peroxidase (HRP)[15] or hemoglobin (Hb)[16] on Au nanoparticles that were attached to gold electrodes by cysteamine chain, and the direct electron transfer for HRP or Hb was observed. A gold nanoparticle-attached indium tin oxide (ITO) electrode was also used to immobilize myoglobin (Mb).[17] The direct electrochemistry of Mb was observed by the well-behaved CV responses for the cast Mb films on ITO/Au electrodes. Ju and coauthors described the direct electrochemical behaviors of Cyt *c*,[18] HRP,[19] Mb,[20] and Hb[21] adsorbed on colloidal gold modified carbon paste electrodes, and studied their electrocatalytic properties toward various substrates. Willner and co-workers[22] fabricated ordered and multilayered films of microperoxidase-11 (MP-11) and Au nanoparticles by covalent cross-link on ITO electrodes. MP-11 in the layer-by-layer constructed MP-11/Au films demonstrated a pair of nearly reversible CV peaks and acted as an electrocatalyst for the reduction of hydrogen peroxide. Recently, Au nanoparticles functionalized with the flavin adenine dinucleotide (FAD)[23] and pyrroloquinoline quinone

* Corresponding author: Fax: (+86) 10−5880−2075. E-mail: hunaifei@bnu.edu.cn.
† Beijing Normal University.
‡ Fuyang Teachers College.

10.1021/jp055301f CCC: $33.50
Published on Web 01/17/2006

(PQQ)[24] cofactors were employed respectively for the reconstitution of apo-glucose oxidase (GOD) and apo-glucose dehydrogenase (GDH) enzymes on electrode surfaces by Willner and co-workers. Highly effective electrical contacting of the enzymes with the electrode was achieved using these nanosized Au particles as electrical connectors. Although the complete understanding for the enhancement of Au nanoparticles on the direct electron transfer of redox proteins has not been very clear yet, some unique properties of Au colloids are most probably related to the effect:[13] (1) The good biocompatibility of colloidal Au is helpful for the attached proteins or enzymes to retain their native structure and enzymatic activity. (2) The high surface-to-volume ratio and corresponding high surface energy of Au nanoparticles result in the strong interaction between proteins and gold colloids, which may allow the protein molecules to orientate in a more favorable fashion on Au surface and shorten the distance between the electroactive prosthetic groups of proteins and Au nanoparticles. (3) The good conductivity of small Au colloids allows them to act as "electron antennas", which may efficiently tunnel electrons between the proteins and electrodes.[14]

By now, most studies on the direct electron transfer of proteins in the films involving Au colloids are concentrated on the protein monolayer[15,16] or cast protein films.[17] In the meantime, covalent binding is usually used in constructing the films containing Au nanoparticles and proteins, including the fabrication of MP-11/Au layer-by-layer films.[22] To the best of our knowledge, no electrostatic layer-by-layer assembly of redox proteins with Au colloids and the corresponding electrochemical study has been reported until now. In the present work, the alternate adsorption of negatively charged Au nanoparticles and positively charged Mb on electrode surface was used to assemble $\{Au/Mb\}_n$ layer-by-layer films through the electrostatic attraction between them. The direct electrochemistry of Mb at $\{Au/Mb\}_n$ film electrodes was studied and was used to electrocatalyze the reduction of oxygen and hydrogen peroxide. Various techniques were employed to monitor the growth of $\{Au/Mb\}_n$ films and characterize the films. Comparative studies of $\{Au/Mb\}_n$ films with other Mb layer-by-layer films assembled with nonconductive nanoparticles or polyions were performed. In particular, the size effect of gold nanoparticles on the electrochemical and biocatalytic activity of $\{Au/Mb\}_n$ films was investigated in detail.

2. Experimental Section

2.1. Reagents. Horse heart myoglobin (Mb, MW 17800) purchased from Sigma was used as received without further purification. Poly(diallyldimethylammonium) (PDDA) and $HAuCl_4 \cdot 3H_2O$ were from Aldrich. Hydrogen peroxide (H_2O_2, 30%) was from Beijing Chemical Engineering Plant. All other chemicals were reagent grade. Phosphate buffer solutions (0.1 M, containing 0.05 M KBr) at pH 7.0 were used as supporting electrolytes for electrochemical experiments. $Fe(CN)_6^{3-/4-}$ solutions (5 mM, containing 0.1 M KCl) with equal concentration of $Fe(CN)_6^{3-}$ and $Fe(CN)_6^{4-}$ were prepared as electrochemical probes. All solutions were prepared with twice-distilled water.

2.2. Apparatus. Electrochemical measurements were performed with a CHI 621B or CHI 660A electrochemical workstation (CH Instruments) using a basal plane pyrolytic graphite (PG, Advanced Ceramics, geometric area 0.16 cm^2) disk modified with films as the working electrode, a saturated calomel electrode (SCE) as the reference electrode, and a Pt flake as the counter electrode. Buffers were purged with highly purified nitrogen for at least 10 min prior to a series of electrochemical experiments. Electrochemical impedance spectroscopy (EIS) measurements were made in the frequency range from 100 kHz to 100 mHz with frequencies logarithmically spaced (10 points per decade) using a 5 mV peak to peak sinusoidal perturbation with the electrode held at the DC formal potential of $Fe(CN)_6^{3-/4-}$ (0.17 V vs SCE).

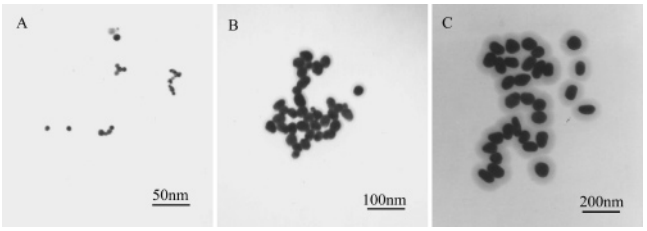

Figure 1. TEM of Au nanoparticles with size of (A) 6, (B) 40, and (C) 90 nm.

Quartz crystal microbalance (QCM) experiments were carried out with a CHI 420 electrochemical analyzer (CH Instruments). Using the Sauerbrey equation[25] and taking into account the properties of the quartz resonator used in this work, the relationship between adsorbed mass, ΔM (g), and frequency shift, ΔF (Hz), is expressed as

$$\Delta F = -7.40 \times 10^8 \Delta M \quad (1)$$

The QCM data were also used to estimate the nominal thickness of adsorbed layer, d (cm), which can be expressed by[5]

$$d = \frac{\Delta M}{2\rho A} \quad (2)$$

where ρ is the density of the film material (g cm^{-3}) and A is the area of Au QCM electrodes (0.196 cm^2). For Mb, the density is $\sim 1.3 \pm 0.1$ g cm^{-3}.[26] Since gold is coated on both sides of the QCM resonator, the total mass adsorbed on the Au electrode should be divided by two. Combining eqs 1 and 2, the relationship between d and ΔF would be

$$d = (-3.4 \times 10^{-9}) \Delta F/\rho \quad (3)$$

UV−vis absorption spectroscopy was done with a Cintra 10e spectrophotometer (GBC). Transmission electron microscopy (TEM) experiments were performed with an H-600 electron microscope (Hitachi). All experiments were performed at ambient temperature (18 ± 2 °C).

2.3. Preparation of Au Colloids. The gold colloids with different sizes were prepared according to the literature.[27−29] In brief, colloidal gold particles with ca. 40 or 90 nm diameter were prepared by adding 0.5 or 0.2 mL of trisodium citrate (1%) into 50 mL of boiling $HAuCl_4$ solution (0.01%) with vigorous stirring. For preparation of Au colloids with size of ca. 6 nm, 50 mL of $HAuCl_4$ solution (0.01%) was heated to boiling, followed by addition of the mixture of 0.2 mL of trisodium citrate (1%) and 0.075 mL of fresh $NaBH_4$ solution (0.075%). The dispersions of Au colloids were kept boiling for 5 min. After cooling, the dispersions were stored at 4 °C and used directly for the preparation of multilayer films. According to TEM (Figure 1), some of the Au nanoparticles had an oval shape, especially for 90 nm Au, but others were essentially spherical. The average diameters of Au colloids were estimated by TEM to be 6, 40, and 90 nm, respectively, with the RSD of 10−25%.

2.4. Film Assembly. For electrochemical studies, the PG electrode was first immersed into PDDA solution (3 mg mL^{-1}, containing 0.5 M NaCl) for 20 min to adsorb positively charged

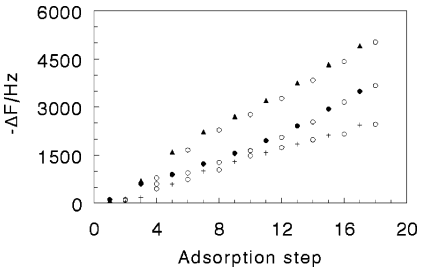

Figure 2. QCM frequency shift with alternate adsorption step for {Au/Mb}$_n$ films with different size of Au nanoparticles on Au/MPS/PDDA surface: (+) 6 nm Au, (●) 40 nm Au, (▲) 90 nm Au, and (○) Mb.

PDDA as a precursor layer. The electrode was then alternately immersed for 20 min in as-prepared Au colloid dispersion and Mb solution (1 mg mL^{-1} at pH 5.0) with intermediate water washing and nitrogen stream drying, forming an Au/Mb bilayer. This cycle was repeated to obtain the desired number of bilayers (n) for {Au/Mb}$_n$ layer-by-layer films.

For QCM studies, the gold QCM resonator electrode (geometric area 0.196 cm^2, fundamental frequency 8 MHz) was first pretreated with piranha solution. (*Caution!* the piranha solution is highly corrosive and should be handled with extreme care. Only a small volume should be prepared at any time.) After thorough water washing, the gold electrode was immersed into 3-mercapto-1-propanesulfonate (MPS, Aldrich) solution (4 mM) for 24 h. MPS was chemisorbed on gold surface, making the surface become negatively charged. A PDDA precursor layer and subsequent {Au/Mb}$_n$ films were then assembled on the Au/MPS surface with the same way as on PG electrodes. After each adsorption step, the resonator was washed with water, dried under nitrogen stream, and the frequency was measured in air. For UV−vis spectroscopy, the quartz slide (0.8 × 4 cm, 1 mm thick) was pretreated with piranha solution, and PDDA/{Au/Mb}$_n$ films were then assembled with the same method as on PG electrodes.

3. Results

3.1. Assembly of {Au/Mb}$_n$ Layer-by-Layer Films. Gold nanoparticles prepared by reaction of $HAuCl_4$ with trisodium citrate possess negative charges.[30] Mb, with its isoelectric point at 6.8,[31] has net positive surface charges at pH 5.0. Thus, oppositely charged Au colloids and Mb could form {Au/Mb}$_n$ layer-by-layer films on solid substrates, such as gold QCM electrodes, PG electrodes, and quartz slides, mainly by electrostatic interaction between them. The assembly process of the layer-by-layer films was monitored by QCM, EIS, and CV.

For QCM studies, a roughly linear decrease in frequency with adsorption step was observed for {Au/Mb}$_n$ films assembled with different sizes of gold nanoparticles (Figure 2), indicating that for a specific system, the adsorption amounts of Mb or Au in each adsorption bilayer are nearly the same, and the growth of {Au/Mb}$_n$ films is uniform and regular. The QCM results for the three types of {Au/Mb}$_n$ films are also listed in Table 1 for comparison. For example, the average decrease in frequency caused by the adsorption of Au nanoparticle layer was 283 Hz for {Au(6 nm)/Mb}$_n$ films, 319 Hz for {Au(40 nm)/Mb}$_n$ films, and 554 Hz for {Au(90 nm)/Mb}$_n$ films, showing a sequence of 6 nm < 40 nm < 90 nm. This is understandable since a larger Au nanoparticle has a greater mass, and its adsorption results in larger decrease in QCM frequency. However, the frequency decrease caused by each Mb adsorption layer displayed a reverse sequence of 6 nm > 40 nm > 90 nm for the three types of {Au/Mb}$_n$ films, suggesting that the amount of Mb adsorbed on the surface of smaller-sized gold nanoparticles is greater than that of larger-sized ones. For {Au/Mb}$_n$ films with three different size of Au nanoparticles, the nominal thickness of each Mb layer estimated by QCM was in the range of 2.6−3.7 nm (Table 1), roughly consistent with the dimension of Mb (2.5 × 3.5 × 4.5 nm^3 [32]) and showing the approximate monolayer adsorption of Mb. Since the information on the density of Au colloids is not available, it is difficult to quantitatively estimate the nominal thickness of Au adsorption layers and the relative surface coverage of Au colloids compared with the ideal monolayer adsorption. However, the qualitative or semiquantitative comparison between differently sized Au nanoparticles could be made from the QCM results. The relative surface coverage of adsorbed Au nanoparticles showed a sequence of 6 nm > 40 nm > 90 nm, and the surface coverage for 6 nm Au was about 5.8 and 7.4 times larger than that for 40 and 90 nm Au, respectively.

EIS was employed to monitor the growth of {Au/Mb}$_n$ films with the redox probe of $Fe(CN)_6^{3-/4-}$ at its formal potential (0.17 V vs SCE). Figure 3A shows the impedance spectra in the form of Nyquist diagrams at the {Au(6 nm)/Mb}$_n$ film electrodes with different number of bilayers (n). The typical semicircles were observed for the {Au(6 nm)/Mb}$_n$ films in EIS responses, showing that the layer-by-layer buildup of the films had a marked influence on their EIS responses. The diameter of the semicircle usually equals the electron-transfer resistance (R_{ct}), which controls the electron-transfer kinetics of the redox probe at the electrode interface.[33] The values of R_{ct} could be estimated by using the Randles equivalent circuit[34,35] as the model and fitting the impedance data into the model. The R_{ct} values showed a nearly linear increase with n for {Au/Mb}$_n$ films with all three sizes of Au nanoparticles (Figure 3B), suggesting a uniform growth of the films in the assembling process.

CV was also used to monitor the growth of {Au/Mb}$_n$ films. Taking {Au(90 nm)/Mb}$_n$ films as an example (Figure 4A), both reduction and oxidation peak currents centered at about −0.35 V vs SCE increased nonlinearly with the number of bilayers (n) up to 13, and then reached a steady state, indicating that the gold nanoparticles and Mb have been successfully assembled layer-by-layer on the surface of PG electrodes at least when n < 14. All three types of {Au/Mb}$_n$ films with different size of Au nanoparticles demonstrated similar growth behavior (Figure 4B). To further confirm the assembly of {Au/Mb}$_n$ layer-by-layer films, the control experiment was conducted, in which the solution of trisodium citrate (1%) containing no Au nanoparticles was used to replace the colloidal Au dispersion in the assembly of Mb layer-by-layer films on PG/PDDA surface, and CVs were performed for the films. While the CV peaks of Mb in these films were also observed at about −0.35

TABLE 1: QCM Results of Each Adsorption Layer for {Au/Mb}$_n$ Films with Different Sizes of Au Nanoparticles

	$-\Delta F$ (Hz)		$\Delta M/A$ (ng cm^{-2})			
films	Au	Mb	Au	Mb	d (nm) for Mb	Γ (mol cm^{-2}) for Mb
{Au(6 nm)/Mb}$_n$	283 ± 23	142 ± 18	1951	979	3.72	5.5×10^{-11}
{Au(40 nm)/Mb}$_n$	319 ± 44	126 ± 66	2198	867	3.29	4.9×10^{-11}
{Au(90 nm)/Mb}$_n$	554 ± 95	98 ± 26	3820	676	2.56	3.8×10^{-11}

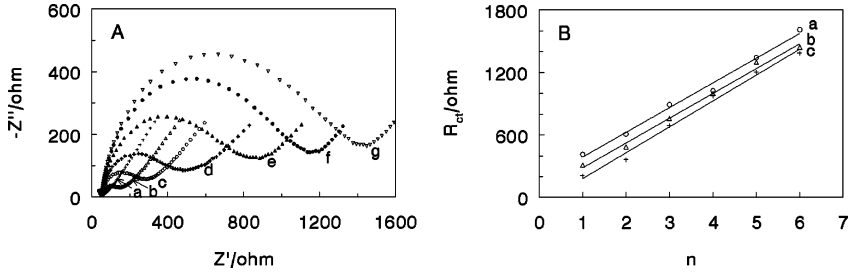

Figure 3. (A) EIS responses of (a) 6 nm Au nanoparticle films and (b−g) {Au(6 nm)/Mb}$_n$ films with $n = 1-6$ in 5 mM $Fe(CN)_6^{3-/4-}$ solutions. (B) Influence of n on R_{ct} for {Au/Mb}$_n$ films with diameter of Au nanoparticles of (a) 90, (b) 40, and (c) 6 nm.

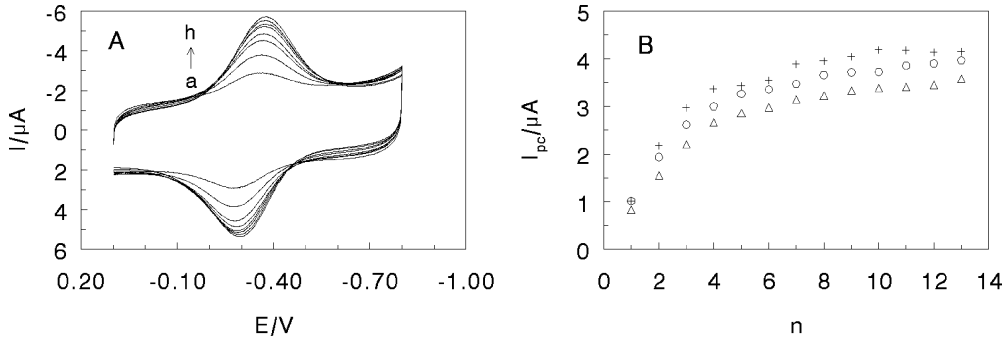

Figure 4. (A) Cyclic voltammograms at 0.2 V s^{-1} in pH 7.0 buffers for {Au(90 nm)/Mb}$_n$ films assembled on PG/PDDA electrodes. The number of bilayers (n): (a) 1, (b) 2, (c) 3, (d) 4, (e) 5, (f) 7, (g) 10, and (h) 13. (B) Dependence of reduction peak current on the number of bilayers (n) for {Au/Mb}$_n$ films with different size of Au nanoparticles: (+) 6, (○) 40, and (△) 90 nm.

V, they essentially did not increase with the number of bilayers, and they were much smaller than those of corresponding {Au/Mb}$_n$ films. The prerequisite to realize the electrostatic layer-by-layer assembly is the charge reversal in each adsorption step.[5] Compared with the polyions, nanoparticles, or proteins, which all carry a lot of charges on their surface, a small ion such as citrate has only a very limited number of charges, and it usually is unable to realize the charge reversal in adsorption.

3.2. Voltammetric Properties. CVs of {Au/Mb}$_n$ films demonstrated a pair of well-defined, nearly reversible peaks at about −0.35 V, characteristic of Mb heme Fe^{III}/Fe^{II} redox couples (e.g., Figure 4A). When $n = 13$, the peak currents reached the steady state and essentially no longer increased with n, the {Au/Mb}$_{13}$ films with $n = 13$ were thus used for the following voltammetric studies. For the {Au/Mb}$_{13}$ films, the CV peak shapes were nearly symmetrical, and the reduction and oxidation peak currents were roughly equal. Both reduction and oxidation peak currents increased linearly with scan rates in the range from 0.05 to 2.0 V s^{-1}. All these results indicate that the {Au/Mb}$_{13}$ films behave as the typical surface-confined or thin-layer voltammetric system.[36] In this kind of system, the surface concentration of electroactive proteins (Γ^*) can be estimated by integration of CV reduction peak and applying the equation of $Q = nFA\Gamma^*$,[36] where Q is the charge (C) passing through the electrode with full reduction of electroactive Mb in the films, A is the area of the electrode (0.16 cm^2), and n and F have their usual meaning. The Γ^* values and other voltammetric parameters for {Au/Mb}$_{13}$ films with different size of Au nanoparticles are listed in Table 2 for comparison. Both the surface concentration of electroactive Mb (Γ^*) and CV peak currents showed a sequence of 6 nm > 40 nm > 90 nm. This sequence is consistent with that of surface concentration of Mb (Γ) adsorbed in each bilayer estimated by QCM (Table 1), suggesting that the {Au/Mb}$_{13}$ films with smaller-sized Au colloids not only have larger total amounts of adsorbed Mb in the assembly, but also have greater surface concentration of electroactive Mb in the films.

TABLE 2: Electrochemical Properties of {Au/Mb}$_{13}$ Films and Other Mb Layer-by-Layer Films Estimated by CV at 0.2 V s^{-1} in pH 7.0 Buffers

films	$E^{\circ\prime}$ (V)	ΔE_p (V)	Γ^*_{max} (mol cm^{-2})	ref
{Au(6 nm)/Mb}$_{13}$	−0.352	0.092	2.92×10^{-10}	this work
{Au(40 nm)/Mb}$_{13}$	−0.353	0.096	2.72×10^{-10}	this work
{Au(90 nm)/Mb}$_{13}$	−0.356	0.104	2.33×10^{-10}	this work
{SiO_2/Mb}$_6$	−0.319	0.085	2.29×10^{-10}	11
{PSS/Mb}$_6$	−0.341	0.107	1.32×10^{-10}	37

After reaching the steady state, the CV peak currents of Mb layer-by-layer films did not increase with the number of bilayers any more, the maximum surface concentration of electroactive Mb (Γ^*_{max}) in the films was thus obtained. If n_{max} is defined as the number of bilayers when the steady-state begins to reach, different types of Mb multilayer films would have different values of n_{max}. For example, while the n_{max} value of {Au/Mb}$_n$ films could extend to 13, the {SiO_2/Mb}$_n$[10,11] and {PSS/Mb}$_n$[37] films showed the n_{max} value at only about 6, where SiO_2 represents silica nanoparticles and PSS stands for poly(styrenesulfonate). All Γ^*_{max} values for three {Au/Mb}$_n$ films with different sizes of Au colloids were larger than that of {SiO_2/Mb}$_n$ or {PSS/Mb}$_n$ films (Table 2). In addition, unlike the {SiO_2/Mb}$_6$ and {PSS/Mb}$_6$ films, the {Au/Mb}$_{13}$ films showed no change of CV peak separation ($\Delta E_p = E_{pa} - E_{pc}$) with increase of scan rate, indicating better electrochemical reversibility of Mb in {Au/Mb}$_{13}$ films.

For {Au(6 nm)/Mb}$_n$ films, the Γ^* value for the first bilayer was estimated to be 5.4×10^{-11} mol cm^{-2}, while the average surface concentration of total adsorbed Mb in each bilayer (Γ) was about 5.5×10^{-11} mol cm^{-2} according to the QCM data (Table 1). The approximate agreement between Γ^* and Γ values suggests that almost all Mb molecules in the first bilayer closest to the electrode surface is electroactive. The fraction of electroactive Mb or the ratio of Γ^*/Γ in the following bilayers was thus estimated for {Au(6 nm)/Mb}$_n$ and other {Au/Mb}$_n$ films. The Γ^*/Γ ratio decreased with the number of bilayers (n) for all {Au/Mb}$_n$ films (Figure 5). However, the decrease

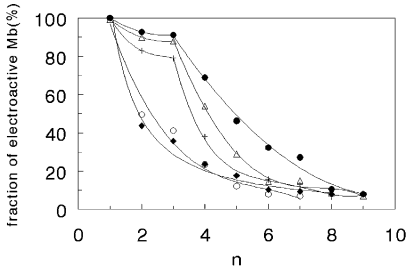

Figure 5. Influence of the number of bilayers (*n*) on the fraction of electroactive Mb for (●) {Au(6 nm)/Mb}$_n$, (△) {Au(40 nm)/Mb}$_n$, (+) {Au(90 nm)/Mb}$_n$, (○) {SiO_2/Mb}$_n$, and (◆) {PSS/Mb}$_n$ films.

trend of {Au/Mb}$_n$ films was different with that of {SiO_2/Mb}$_n$ and {PSS/Mb}$_n$ films (Figure 5). Compared with {SiO_2/Mb}$_n$ or {PSS/Mb}$_n$ films, in which the Γ*/Γ ration reached to zero when *n* approached to 7, the {Au/Mb}$_n$ films showed a much slower decrease trend in the fraction of Γ*/Γ, which reached to zero when *n* equaled to 14.

3.3. EIS Behaviors. EIS was employed to study the conductivity of gold nanoparticles using $Fe(CN)_6^{3-/4-}$ as the redox probe (Figure 6A). When PDDA/PSS/PDDA layers were successively adsorbed on the surface of PG electrodes, the EIS response in the Nyquist plot showed an obvious difference than that at bare PG electrodes. Compared with the straight-line shape in response for bare PG, the semicircle-like shape with large diameter was observed for PDDA/PSS/PDDA layers, indicating that the adsorption layers lead to a great increase in resistance. However, when Au nanoparticles (6 nm) were adsorbed on the PDDA/PSS/PDDA surface, the electron-transfer resistance (R_{ct}) decreased from 437 to 81 Ω (Figure 6A). The adsorption of Au nanoparticles "compensated" the R_{ct} increase caused by the PDDA/PSS/PDDA adsorption due to the better conductivity of Au colloids. This viewpoint was further confirmed by CV experiments with $Fe(CN)_6^{3-/4-}$ couple (Figure 6B), in which the peak-to-peak separation increased from 0.112 to 0.274 V after PDDA/PSS/PDDA layers were adsorbed on the bare PG electrode, and then decreased to 0.230 V when the 6 nm-gold nanoparticles were further adsorbed, suggesting the enhancement of electron transfer by Au colloids. Both reduction and oxidation peak currents of $Fe(CN)_6^{3-/4-}$ for PDDA/PSS/PDDA/Au layers were larger than those for PDDA/PSS/PDDA layers, also indicating the effect of Au colloids in improvement of film conductivity. Considering that the PDDA outerlayer has positive charges, which would be beneficial to attract negatively charged $Fe(CN)_6^{3-/4-}$, while the Au nanoparticles have negative surface charges, which would have strong repulsive interaction with $Fe(CN)_6^{3-/4-}$, the enhancement of Au nanoparticles for the electron transfer of $Fe(CN)_6^{3-/4-}$ would be more impressive. Here, the three-layered film of PDDA/PSS/PDDA instead of PDDA monolayer was used because the R_{ct} value of the PDDA/PSS/PDDA film was much larger than that of the PDDA monolayer. Thus, the difference in EIS and CV responses between bare PG and the PDDA/PSS/PDDA film became more pronounced, and the conducting effect of Au nanoparticles was observed more obviously.

The conductivity of Au nanoparticles was also tested by comparative EIS experiments of {Au/Mb}$_6$ films with {SiO_2/Mb}$_6$ and {PSS/Mb}$_6$ films, setting the number of bilayers (*n*) at the same value of 6 (Figure 7). The results showed that the R_{ct} value of all three {Au/Mb}$_6$ films with different size of Au nanoparticles were smaller than that of either {SiO_2/Mb}$_6$ or {PSS/Mb}$_6$ films, suggesting that the enhancement effect of Au nanoparticles for the electron transfer of redox probes in the layer-by-layer films is better than that of nonconductive nanoparticles or polyelectrolytes. In addition, for the same type of {Au/Mb}$_6$ films but with different size of Au nanoparticles, the R_{ct} value displayed a sequence of 6 nm < 40 nm < 90 nm (Figure 7), demonstrating that the Au nanoparticles with smaller size have better conductivity than those with larger size.

3.4. Catalytic Reactivity. Electrocatalytic reduction of oxygen at {Au/Mb}$_n$ film electrodes was examined by CV. Take {Au(6 nm)/Mb}$_{13}$ films as an example (Figure 8A). The direct reduction of oxygen at gold nanoparticle film electrodes was observed at about −0.45 V, while Mb in {Au/Mb}$_{13}$ films allowed the reduction peak potential of oxygen to shift positively to −0.35 V. With the same amount of air passing through the buffers, the reduction peak current at {Au(6 nm)/Mb}$_{13}$ films was much larger than that at Au nanoparticle films alone (Figure 8A, curves e and b). Compared with {Au(6 nm)/Mb}$_{13}$ films in the absence of oxygen, the presence of oxygen resulted in a great increase of reduction peak current, and a decrease or even disappearance of oxidation peak. The reduction peak current increased with the amount of oxygen. Catalytic efficiency, expressed as the ratio of reduction peak current in the presence (I_c) and absence of oxygen (I_d), I_c/I_d, decreased with increase of scan rate (Figure 8B). All these results suggest that oxygen is catalytically reduced at {Au/Mb}$_{13}$ film electrodes. Under the same conditions, the catalytic efficiency of {Au/Mb}$_{13}$ films with different size of Au nanoparticles showed a sequence of 6 nm > 40 nm > 90 nm (Figure 8B).

Catalytic reduction of hydrogen peroxide at {Au/Mb}$_{13}$ film electrodes was also studied by CV. Taking {Au(6 nm)/Mb}$_{13}$ films as an example (Figure 9A), when H_2O_2 was added into the buffer solution, the reduction peak greatly increased while the oxidation peak decreased. The reduction peak current increased linearly with the concentration of H_2O_2 within a certain range. The catalytic CV behavior of H_2O_2 at {Au/Mb}$_{13}$ films was very similar to that of O_2, indicating the similar catalytic mechanism of two systems as described previously for other Mb film systems.[38]

The electrocatalytic reduction of H_2O_2 at {Au/Mb}$_{13}$ films was also tested by amperometry. The typical amperometric current−time plots for {Au/Mb}$_{13}$ films showed that with the

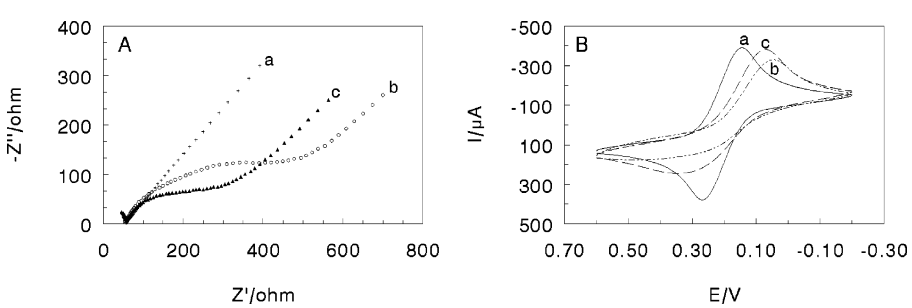

Figure 6. (A) EIS and (B) CV responses of (a) bare PG electrode, (b) PDDA/PSS/PDDA films on PG, and (c) PDDA/PSS/PDDA/Au(6 nm) films on PG in 5 mM $Fe(CN)_6^{3-/4-}$ solutions.

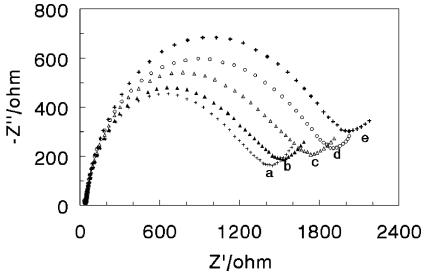

Figure 7. EIS responses for (a) $\{Au(6\ nm)/Mb\}_6$, (b) $\{Au(40\ nm)/Mb\}_6$, (c) $\{Au(90\ nm)/Mb\}_6$, (d) $\{SiO_2/Mb\}_6$, and (e) $\{PSS/Mb\}_6$ film modified electrodes in 5 mM $Fe(CN)_6^{3-/4-}$ solutions.

stepwise addition of H_2O_2 at the constant potential of −0.1 V vs SCE, the corresponding increase of currents was observed (Figure 9B). While gold nanoparticle films without Mb also displayed some catalytic activity toward H_2O_2 reduction in amperometry, $\{Au/Mb\}_{13}$ films behaved much better. The increase of current had a linear relationship with the concentration of hydrogen peroxide for all three $\{Au/Mb\}_{13}$ films with different size of Au nanoparticles. However, the slope of calibration curve showed a sequence of 6 nm > 40 nm > 90 nm, in agreement with the sequence of Γ and Γ*. Catalytic performances of $\{Au/Mb\}_{13}$ films with different size of Au nanoparticles toward the reduction of oxygen and hydrogen peroxide are listed in Table 3 for comparison.

The influence of the number of bilayers (n) on the catalytic efficiency (I_c/I_d) of H_2O_2 for $\{Au/Mb\}_n$ films was also investigated. The results showed that the $\{Au/Mb\}_n$ films with a larger n value may not always lead to a larger ratio of I_c/I_d. For example, for $\{Au(40\ nm)/Mb\}_n$ films, the ratio of I_c/I_d for 20 μM H_2O_2 at 0.2 V s^{-1} in pH 7.0 buffers was 2.32 at $n = 3$, a little smaller than 2.44 at $n = 6$, but all of them were larger than 1.57 when $n = 13$. While the $\{Au/Mb\}_{13}$ films with $n = 13$ had the larger amount of electroactive Mb, which would be beneficial to the electrocatalytic reduction of H_2O_2, the thicker films would increase the transportation resistance of H_2O_2 through the films, which would restrict the effective contact of the substrate with the protein and thus decrease the catalytic efficiency. These two opposite influencing factors may impose together on the electrocatalysis, and make the appearance of a maximum catalytic efficiency at a medium n value.

3.5. Conformational Studies. The position of Soret band of heme proteins caused by the heme prosthetic group may provide conformational information on the proteins, especially in the heme region,[39] UV−vis spectroscopy was thus used to investigate the possible denaturation of Mb in $\{Au/Mb\}_8$ films assembled on quartz slides. Results showed that the Soret band of Mb in all three $\{Au/Mb\}_8$ films with different size of Au nanoparticles in their dry form was located at the same position of 408 nm, same as that of Mb solution and dry Mb films alone (Table 4). When the $\{Au/Mb\}_8$ films were placed in buffers at pH 5.0 or 7.0, the Soret band was still observed at 408 nm. These results indicate that Mb in $\{Au/Mb\}_8$ films essentially retain its native structure in both dry and "wet" form at medium pH.

Au nanoparticles with diameter of about 10 nm in their aqueous dispersions have a strong surface plasmon absorption band at about 520 nm, and the band shows a red-shift when the size of Au nanoparticles increases.[12] This was confirmed by our experiments (Table 4), in which the peak at 519 nm for 6 nm diameter Au colloids in their dispersion red-shifted to 526 nm for 40 nm Au and 542 nm for 90 nm Au. Dry $\{Au/Mb\}_n$ films also showed the surface plasmon absorption band for Au with a longer wavelength than Au nanoparticles in dispersion (Table 4). For example, with the same size of 40 nm, $\{Au(40\ nm)/Mb\}_n$ films showed the absorption band at 545 nm, about 19 nm longer than that of 40 nm diameter Au nanoparticles in dispersion. This result was also observed in other Au nanoparticle films[40] and explained by the aggregation of Au nanoparticles in the film formation. The change of dielectric environ-

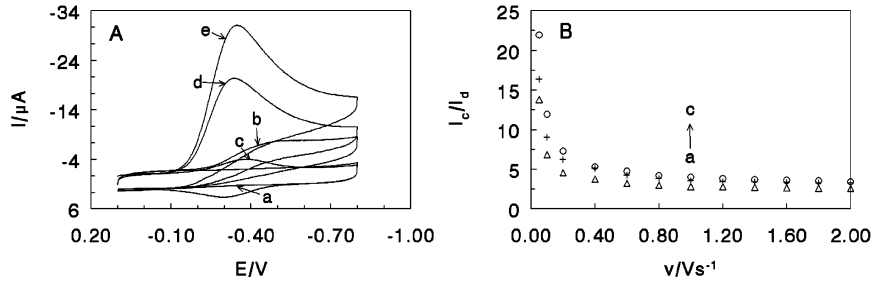

Figure 8. (A) Cyclic voltammograms at 0.2 V s^{-1} in 10 mL of pH 7.0 buffers for (a) 6 nm Au nanoparticle films, (b) 6 nm Au nanoparticle films after 40 mL of air was injected, (c) $\{Au(6\ nm)/Mb\}_{13}$ films, (d) $\{Au(6\ nm)/Mb\}_{13}$ films with 20 mL of air, and (e) $\{Au(6\ nm)/Mb\}_{13}$ films with 40 mL of air. (B) Influence of scan rate (v) on catalytic efficiency (I_c/I_d) for (a, Δ) $\{Au(90\ nm)/Mb\}_{13}$, (b, +) $\{Au(40\ nm)/Mb\}_{13}$, and (c, ○) $\{Au(6\ nm)/Mb\}_{13}$ films in pH 7.0 buffers, where I_d is the CV reduction peak current in the buffers without oxygen and I_c is the CV reduction peak current in 10 mL buffers after 40 mL of air was injected.

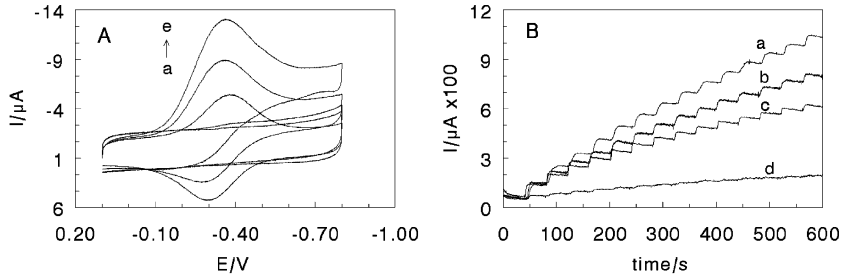

Figure 9. (A) Cyclic voltammograms at 0.2 V s^{-1} in 10 mL of pH 7.0 buffers for (a) 6 nm Au nanoparticle films, (b) 6 nm Au nanoparticle films in the presence of 10 μM H_2O_2, (c) $\{Au(6\ nm)/Mb\}_{13}$ films, (d) $\{Au(6\ nm)/Mb\}_{13}$ films with 10 μM H_2O_2, and (e) $\{Au(6\ nm)/Mb\}_{13}$ films with 20 μM H_2O_2. (B) Amperometric responses of (a) $\{Au(6\ nm)/Mb\}_{13}$ films, (b) $\{Au(40\ nm)/Mb\}_{13}$ films, (c) $\{Au(90\ nm)/Mb\}_{13}$ films, and (d) 6 nm Au nanoparticle films at −0.1 V in pH 7.0 buffers with injecting 10 μM H_2O_2 every 40 s.

TABLE 3: Catalytic Performances of $\{Au/Mb\}_{13}$ Films toward Reduction of Oxygen and Hydrogen Peroxide

substrates		$\{Au/Mb\}_{13}$ films 6 nm	40 nm	90 nm
O_2[a]	catalytic efficiency (I_c/I_d)	21.95	16.38	13.76
H_2O_2[b] (CV)	catalytic efficiency (I_c/I_d)[d]	2.04	1.57	1.38
	linear range (μM)	0.6−80	0.7−90	1.0−70
	correlation coeff	0.999	0.999	0.997
	sensitivity (A M^{-1} cm^{-2})	0.812	0.750	0.638
	detection limit (μM)	0.4	0.4	0.4
H_2O_2[c] (amperometry)	linear range (μM)	1.2−90	1.2−90	2.0−80
	correlation coeff	0.998	0.999	0.998
	sensitivity (A M^{-1} cm^{-2})	0.476	0.352	0.311
	detection limit (μM)	0.4	0.4	1.2

[a] CV, at 0.05 V s^{-1} in 10 mL of pH 7.0 buffers with 40 mL of air injected. [b] 0.2 V s^{-1} in pH 7.0 buffers. [c] At −0.1 V in 10 mL of pH 7.0 buffers. [d] 20 μM H_2O_2.

TABLE 4: Wavelengths of Surface Plasmon Band of Au and Soret Band of Mb by UV−Vis Spectroscopy

absorption band type	systems	size of Au nanoparticles (nm) 6	40	90
surface plasmon band of Au	colloidal Au	519	526	542
	$\{Au/Mb\}_8$ films	545	545	552
Soret band of Mb	dry $\{Au/Mb\}_8$ films	408	408	408
	$\{Au/Mb\}_8$ films at pH 5.0	408	408	408
	$\{Au/Mb\}_8$ films at pH 7.0	408	408	408
	Mb solution		408	
	dry Mb film		408	

ment of gold nanoparticles when the films were assembled with proteins may also result in the red shift in absorption.[41]

4. Discussion

Gold nanoparticles, with their good biocompatibility and conductivity, can form various films with redox proteins on electrode surface, in which the proteins retain their native structure and demonstrate direct electrochemistry.[13] Different kinds of protein films involving gold nanoparticles provide a favorable microenvironment for the proteins and enhance the electron transfer of the proteins with underlying electrodes. Although the mechanism of the enhancement is not very clear yet, it is thought that gold nanoparticles may penetrate slightly into the redox proteins and approach the electroactive prosthetic groups inside the proteins,[42] or/and the proteins immobilized on colloidal Au surface may take a favored orientation,[43] all lowering the electron-transfer distance between the Au nanoparticles and the redox sites embedded in proteins. In either case, the Au colloids act as a conducting bridge between the redox center of proteins and the electrode surface. The advantages of Au colloids in fabricating redox protein films were also demonstrated by the $\{Au/Mb\}_n$ multilayer films assembled on PG electrodes in the present work. Mb in the films essentially kept its native structure (Table 4), and demonstrated reversible CV responses and good electrocatalytic properties (Figures 4, 8, and 9 and Tables 2 and 3). In particular, compared with other Mb layer-by-layer films such as $\{SiO_2/Mb\}_n$ and $\{PSS/Mb\}_n$ films, $\{Au/Mb\}_n$ films showed smaller electron-transfer resistance (R_{ct}, Figure 7) and larger maximum surface concentration of electroactive Mb (Γ^*_{max}, Table 2), indicating the conducting tunnel effect of colloidal gold in facilitating electron transfer of the protein. The conductivity of Au nanoparticles was further confirmed by the EIS experiments with the $Fe(CN)_6^{3-/4-}$ probe, in which the R_{ct} value was greatly increased when PDDA/PSS/PDDA insulation layers were adsorbed on bare PG electrodes, and then significantly decreased by the following adsorption of Au colloid layer (Figure 6). If the Au nanoparticles were not conductive, the additional adsorption layer of Au colloids with negative charges on PDDA/PSS/PDDA surface would have increased the R_{ct} when using the likely charged $Fe(CN)_6^{3-/4-}$ as the probe. However, the resistance caused by the thicker PDDA/PSS/PDDA/Au layers decreased but not increased compared with the PDDA/PSS/PDDA layers only, demonstrating the conducting effect of Au layer. Similar results were also observed by Oyama et al.[44] and Sun et al.,[45] in which the deposition of gold nanoparticles effectively improved electron-transfer kinetics between $Fe(CN)_6^{3-/4-}$ redox probe and electrodes. It is because of the good conductivity of Au nanoparticles that the electroactivity of Mb in $\{Au/Mb\}_n$ films was extended to 13 bilayers, much larger than that for $\{SiO_2/Mb\}_n$ or $\{PSS/Mb\}_n$ films, in which the SiO_2 nanoparticles or PSS polyelectrolytes were not conductive and the electroactive Mb was only extended to about six bilayers.[10,11,37] Thus, the maximum surface concentration of electroactive Mb (Γ^*_{max}) loaded in $\{Au/Mb\}_n$ films is higher than that for other Mb layer-by-layer films (Table 2). Also, most probably due to the good conductivity of Au nanoparticles, the CV peak separation (ΔE_p) for Mb Fe^{III}/Fe^{II} redox couple at $\{Au/Mb\}_{13}$ film electrodes is independent of scan rate, suggesting an improved reversibility of Mb electrochemistry in this suitable microenvironment.

Like other protein layer-by-layer films, the $\{Au/Mb\}_n$ films grew linearly with nearly constant adsorption amounts of Mb in each bilayer (Figures 2 and 3 and Table 1), but the electroactive Mb could only extend to a limited number of bilayers, suggesting that only the Mb molecules in the first few bilayers closest to the electrode surface are electrochemically addressable. The fraction of electroactive Mb (Γ^*/Γ) decreased with the number of bilayers (n) for $\{Au/Mb\}_n$ and other Mb layer-by-layer films, but the decrease trend was different (Figure 5). The $\{Au/Mb\}_n$ films demonstrated a much slower decrease tendency than $\{SiO_2/Mb\}_n$ or $\{PSS/Mb\}_n$ films. Particularly, for $\{Au/Mb\}_n$ films, the Γ^*/Γ ratio in the first three bilayers kept on a very high level and then declined significantly, while for $\{SiO_2/Mb\}_n$ and $\{PSS/Mb\}_n$ films, the drastic decrease of Γ^*/Γ value was observed from the second bilayer (Figure 5).

All three $\{Au/Mb\}_n$ films assembled with different size of Au nanoparticles showed the same tendency. Taking the $\{Au(6\ nm)/Mb\}_n$ films as an example, the fraction of electroactive Mb remained at a high level of about 90% for both the second and third bilayers, but for $\{SiO_2/Mb\}_n$ films the ratio decreased to about 50% when $n = 2$. This substantial difference may also be ascribed to the good conductivity of Au colloids. The conductive gold nanoparticles seem to play a more crucial role in the first three Au/Mb bilayers in Mb electrochemistry, resulting in a higher fraction of electroactive Mb in these bilayers.

In addition, the presence of relatively high concentration of positively charged amino acid groups around the heme cleft of Mb molecule at pH 5.0 may make the cleft side of Mb face to the negatively charged Au surface in adsorption. This favorable orientation of Mb would greatly shorten the distance between the electroactive heme group of Mb and Au nanoparticle. The suitable orientation of proteins induced by electrostatic interaction, combined with the good conductivity of gold colloids, was also reported to have enhanced the direct electron transfer of Cyt *c* at electrodes modified with Au nanoparticles.[14,46] In the meantime, the $\{Au/Mb\}_n$ films may also have a porous structure like MP-11/Au multilayer films,[22] which allowed the substrates such as H_2O_2 to penetrate into the films and react with Mb. The good permeability and porosity of $\{Au/Mb\}_n$ films may also allow the small counterions in buffers to get into and leave out from the films more easily, which is another important factor in facilitating the direct electrochemistry of proteins in films.[47]

The $\{Au/Mb\}_n$ layer-by-layer films showed advantages over other Mb films involving colloidal Au in Mb electrochemistry. In general, the layer-by-layer assembly is better than cast films in its precise control of the film composition and layer thickness at the nanometer level, than other precisely controlled methods such as self-assembly monolayer (SAM) and Langmuir−Blodgett (LB) membrane in its better flexibility and simplicity. In particular, the $\{Au/Mb\}_n$ layer-by-layer films could load much more amounts of Mb in their multilayered architecture than the other Au nanoparticle-involved Mb monolayer films, giving rise to higher Γ^*_{max} value and better electrocatalytic activity.

The size of colloidal Au showed a significant influence on the assembly of $\{Au/Mb\}_n$ layer-by-layer films and the corresponding electrochemical and electrocatalytic activity. The $\{Au/Mb\}_n$ films assembled with smaller-sized gold colloids loaded larger amounts of Mb in each bilayer (Γ, Figure 2 and Table 1), mainly because the smaller Au particles have higher surface-to-volume ratio and provide more active binding sites on their surface for immobilization of Mb. The $\{Au/Mb\}_n$ films with the same *n* value but different size of Au nanoparticles showed a sequence of 6 nm > 40 nm > 90 nm in both CV peak currents and maximum surface concentration of electroactive Mb (Γ^*_{max}, Figure 4 and Table 2). This is not only attributed to the higher loading of total amounts of Mb in the films with smaller-sized Au, as observed in other protein-loading Au colloid films,[16,48] but also because of the better conductivity and smaller resistance of the films assembled with smaller Au nanoparticles, as illustrated by the electrochemical impedance measurements (Figure 7). The latter factor seems to play a more important role in the Mb electrochemistry. According to Willner and coworkers,[48] the pack of smaller-sized Au colloids is denser than that of larger-sized Au colloids in the formation of adsorption layer, and smaller Au colloids generate more continuous layers while the larger Au nanoparticles form discontinuous metal layer in the assembly. This conclusion is supported by our QCM experiments (Table 1), in which the surface coverage of Au nanoparticles in each adsorption bilayer for 6 nm Au is much larger than that for 40 and 90 nm Au. Similarly, mainly because of the higher loading of electroactive Mb and better conductivity of Au, the $\{Au/Mb\}_n$ films with smaller-sized Au nanoparticles demonstrated better electrocatalytic performances toward the reduction of oxygen and hydrogen peroxide, such as higher catalytic efficiency (I_c/I_d) and better sensitivity (Figures 8 and 9 and Table 3), which is in good agreement with the observation in the literature.[15,29]

5. Conclusion

The oppositely charged myoglobin and different sized gold nanoparticles are successfully assembled into $\{Au/Mb\}_n$ layer-by-layer films by electrostatic interaction between them. Compared with other Mb layer-by-layer films assembled with nonconductive nanoparticles or polyelectrolytes, the $\{Au/Mb\}_n$ films exhibit higher surface concentration of electroactive proteins and better electrocatalytic activity mainly because of the good conductivity of Au colloids. Because of the high biocompatibility of Au nanoparticles, the Mb in $\{Au/Mb\}_n$ films essentially retains its native structure and displays good biocatalytic activity. The size of gold nanoparticles demonstrates distinct influence on the properties of $\{Au/Mb\}_n$ films. The smaller-sized gold nanoparticles provide more active binding sites for Mb adsorption and demonstrate smaller EIS resistance or better conductivity. Thus, the $\{Au/Mb\}_n$ films with smaller-sized Au colloids load more amounts of Mb, demonstrate better electrochemical and biocatalytic activity than those with larger-sized Au nanoparticles. The unique and excellent properties of $\{Au/Mb\}_n$ films may allow the layer-by-layer assembly of proteins with gold nanoparticles to become a general way to fabricate enzyme films useful in practical applications to biosensors and bioreactors.

Acknowledgment. Financial support from the National Natural Science Foundation of China (Grants 20275006 and 20475008) is acknowledged.

References and Notes

(1) Gorton, L.; Lindgren, A.; Larsson, T. D.; Munteanu, F.; Ruzgas, T.; Gazaryan, I. *Anal. Chim. Acta* **1999**, *400*, 91.
(2) Chaplin, M.; Bucke, C. *Enzyme Technology*, Cambridge University Press: Cambridge, U.K., 1990.
(3) Rusling, J. F. In *Protein Architecture: Interfacing Molecular Assemblies and Immobilization Biotechnology*; Lvov, Y., Mohwald, H., Eds.; Marcel Dekker: New York, 2000; pp 337−354.
(4) Decher, G. *Science* **1997**, *277*, 1232.
(5) Lvov, Y. In *Protein Architecture: Interfacing Molecular Assemblies and Immobilization Biotechnology*; Lvov, Y., Mohwald, H., Eds.; Marcel Dekker: New York, 2000; pp 125−166.
(6) Lvov, Y.; Lu, Z.; Schenkman, J. B.; Zu, X.; Rusling, J. F. *J. Am. Chem. Soc.* **1998**, *120*, 4073.
(7) Ariga, K.; Kunitake, T. In *Protein Architecture: Interfacing Molecular Assemblies and Immobilization Biotechnology*; Lvov, Y., Mohwald, H., Eds.; Marcel Dekker: New York, 2000; pp 169−192.
(8) Lvov, Y.; Munge, B.; Giraldo, O.; Ichinose, I.; Suib, S.; Rusling, J. F. *Langmuir* **2000**, *16*, 8850.
(9) Zhou, Y.; Li, Z.; Hu, N.; Zeng, Y.; Rusling, J. F. *Langmuir* **2002**, *18*, 8573.
(10) He, P.; Hu, N.; Rusling, J. F. *Langmuir* **2004**, *20*, 722.
(11) He, P.; Hu, N. *Electroanalysis* **2004**, *16*, 1122.
(12) Daniel, M.-C.; Astruc, D. *Chem. Rev.* **2004**, *104*, 293.
(13) Liu, S.; Leech, D.; Ju, H. *Anal. Lett.* **2003**, *36*, 1.
(14) Brown, K. R.; Fox, A. P. M.; Natan, M. J. *J. Am. Chem. Soc.* **1996**, *118*, 1154.
(15) Xiao, Y.; Ju, H.; Chen, H. *Anal. Biochem.* **2000**, *278*, 22.
(16) Gu, H.; Yu, A.; Chen, H. *J. Electroanal. Chem.* **2001**, *516*, 119.
(17) Zhang, J.; Oyama, M. *J. Electroanal. Chem.* **2005**, *577*, 273.
(18) Ju, H.; Liu, S.; Ge, B.; Lisdat, F.; Shcller, F. W. *Electroanalysis* **2002**, *14*, 141.

(19) Liu, S.; Ju, H. *Anal. Biochem.* **2002**, *307*, 110.
(20) Liu, S.; Ju, H. *Electroanalysis* **2003**, *15*, 1488.
(21) Liu, S.; Ju, H. *Analyst* **2003**, *128*, 1420.
(22) Patolsky, F.; Gabriel, T.; Willner, I. *J. Electroanal. Chem.* **1999**, *479*, 69.
(23) Xiao, Y.; Patolsky, F.; Katz, E.; Hainfeld, J. F.; Willner, I. *Science* **2003**, *299*, 1877.
(24) Zayats, M.; Katz, E.; Baron, R.; Willner, I. *J. Am. Chem. Soc.* **2005**, *127*, 12400.
(25) Sauerbrey, G. *Z. Phys.* **1959**, *155*, 206.
(26) Creighton, T. E., Ed. *Protein Structure, a Practical Approach*; IRL Press: New York, 1990; p 43.
(27) Frens, G. *Nature (Phys. Sci.)* **1973**, *241*, 20.
(28) Grabar, K. C.; Allison, K. J.; Baker, B. E.; Bright, R. M.; Brown, K. R.; Freeman, R. G.; Fox, A. P.; Keating, C. D.; Musick, M. D.; Natan, M. J. *Langmuir* **1996**, *12*, 2353.
(29) Jia, J.; Wang, B.; Wu, A.; Dong, S. *Anal. Chem.* **2002**, *74*, 2217.
(30) Schmitt, J.; Decher, G.; Dressick, W. J.; Brandow, S. L.; Geer, R. E.; Shashidhar, R.; Calvert, J. M. *Adv. Mater.* **1997**, *9*, 61.
(31) Bellelli, A.; Antonini, G.; Brunori, M.; Springer, B. A. *J. Biol. Chem.* **1990**, *265*, 18898.
(32) Kendrew, J.; Phillips, D.; Stone, V. *Nature (London)* **1960**, *185*, 422.
(33) Katz, E.; Willner, I. *Electroanalysis* **2003**, *15*, 913.
(34) Bard, A. J.; Faulkner, L. R. *Electrochemical Methods*, 2nd ed.; Wiley: New York, 2001.
(35) Randles, J. E. B. *Discuss. Faraday Soc.* **1947**, *1*, 11.
(36) Murray, R. W. In *Electroanalytical Chemistry*; Bard, A. J., Ed.; Marcel Dekker: New York, 1984; Vol. 13, pp 191−368.
(37) Ma, H.; Hu, N.; Rusling, J. F. *Langmuir* **2000**, *16*, 4969.
(38) Zhang, Z.; Chouchane, S.; Magliozzo, R. S.; Rusling, J. F. *Anal. Chem.* **2002**, *74*, 163.
(39) George, P.; Hanania, G. I. H. *J. Biochem.* **1953**, *55*, 236.
(40) Grabar, K. C.; Freeman, R. G.; Hommer, M. B.; Natan, M. J. *Anal. Chem.* **1995**, *67*, 735.
(41) He, J.; Valluzzi, R.; Tripathy, S. K. *Chem. Mater.* **1999**, *11*, 3268.
(42) Shipway, A. N.; Lahav, M.; Willner, I. *Adv. Mater.* **2000**, *12*, 993.
(43) Zhao, J.; Henkens, R. W.; Stonehuerner, J.; O'Daly, J. P.; Crumbliss, A. L. *J. Electroanal. Chem.* **1992**, *327*, 109.
(44) Zhang, J.; Oyama, M. *Electrochim. Acta* **2004**, *50*, 85.
(45) Zhang, S.; Wang, N.; Yu, H.; Niu, Y.; Sun, C. *Bioelectrochemistry* **2005**, *67*, 15.
(46) Wang, L.; Wang, E. *Electrochem. Commun.* **2004**, *6*, 49.
(47) Liu, H.; Hu, N. *J. Phys. Chem. B* **2005**, *109*, 10464.
(48) Doron, A.; Katz, E.; Willner, I. *Langmuir* **1995**, *11*, 1313.